Dynamic Aeration for Improved Oxygen Mass Transfer in the Wastewater Treatment Process

Herrmann-Heber, R.; Reinecke, S.; Hampel, U.;

Originally published:

June 2019

Chemical Engineering Journal 386(2020), 122068

DOI: https://doi.org/10.1016/j.cej.2019.122068

Perma-Link to Publication Repository of HZDR:

https://www.hzdr.de/publications/Publ-28180

Dynamic Aeration for Improved Oxygen Mass Transfer in the Wastewater Treatment Process

R. Herrmann-Heber*, S. F. Reinecke* and U. Hampel*, **

* Department of Experimental Thermal Fluid Dynamics, Institute of Fluid Dynamics, Helmholtz Zentrum Dresden-Rossendorf, Bautzner Landstraße 400, 01328 Dresden, Germany
(E-mail: *r.herrmann-heber@hzdr.de; s.reinecke@hzdr.de; u.hampel@hzdr.de)*
** Chair of Imaging Techniques in Energy and Process Engineering, Technische Universität Dresden, Dresden, 01062, Germany (E-mail: *Uwe.Hampel@tu-dresden.de*)

Abstract

Wastewater treatment is responsible for about 1% of the total electric energy consumption in developed countries. The dynamic aeration method, which applies oscillations to the gas flow, shows a high potential for increase of oxygen mass transfer and energy efficiency of the biological wastewater treatment process. We investigated the mass transfer of pulsed aeration modes in comparison to constant flow aeration in a test geometry in a numerical study. The effects of flow rate, pulsation frequency, bubble size and injection depth on mass transfer were studied. Gas was pulsated with a square wave pattern in on/off mode for the application in aeration basins of wastewater treatment plants. A geometry with up to 4 m aeration depth was investigated. The air supply was pulsed with frequencies in the range of 0.1 to 4 Hz. An increase of oxygen mass transfer rate by up to 24% is determined compared to continuous aeration. Moreover, comparable mass transfer rates are achieved for lower gas mass flow rates during pulsation. Thus, air demand in compression and energy consumption can be reduced when dynamic aeration is applied. The oxygen transfer efficiencies derived from the simulations are in good agreement with the experimental results from Alkhalidi et al. (2016).

Highlights

- Dynamic aeration in form of pulsed modes increases the oxygen mass transfer by up to 24%.
- Pulsed modes lead to higher gas hold-up.
- Potential increase of aeration efficiency by 16% using pulsed modes is shown in relevant scales for wastewater treatment.

Keywords

Wastewater aeration; pulsed aeration; oxygen mass transfer; CFD

INTRODUCTION

In developed countries wastewater treatment is responsible for about 1% of the total electric energy consumption (OECD 2016). About 10,000 wastewater treatment plants in Germany consume 4.4 TWh/a to remove nutrients from wastewater (Fricke 2009). As a part of this treatment process, the activated sludge process uses up to 80% of the total energy budget. In this process, the activated sludge is continuously aerated in 4-6 m deep tanks. The generated bubbles rise in the tank while transferring oxygen into the sludge for nutrient-degrading microorganisms. The oxygen mass transfer in aeration basins is affected by a vast number of hydrodynamic parameters such as gas flow rate, hold-up, bubble size and rise velocity. The oxygen utilization in activated sludge with continuous aeration is low. With an aeration depth of 4 – 6 m and a bubble size of 2 - 4 mm (Hasanen et al. 2006), which is common for modern diffusers, less than 50% of the oxygen content of air bubbles is transferred (Motarjemi and Jameson 1978). Dynamic aeration is proposed to improve oxygen mass transfer, oxygen utilization and aeration efficiency. By improving the oxygen mass transfer the gas flow rate in the aeration process can be lowered and the amount of oxygen, which leaves the aeration tank unused is reduced. This can lead to high energy savings in comparison to traditional operation modes.

Dynamic methods to increase mass transfer have been used in chemical processes such as in bubble column reactors (Elbing et al. 2016). An example is the pulsation of bubble columns, where an actuation device directly introduces pulsations or the entire column is subjected to pulsations. A dynamic aeration method with an intended application to bioreactors was investigated with the help of numerical simulations (Jia et al. 2011), where a pulsed gas flow was added to a continuous flow. This showed positive effects on the turbulent kinetic energy and the volumetric mass transfer rate could be increased for specific cases. This was verified in a small scale setup with 0.6 m liquid level (Zhou et al. 2013). With respect to wastewater treatment with flexible membrane diffusers the group of Xu used solenoid valves to pulse the

gas flow to a single membrane diffuser with a pulsation frequency of 10 Hz in a small basin with 1.0 m liquid level (Xu et al. 2015). The group of Alkhalidi connected two diffusers to a gas feed line with one solenoid valve for each of the diffusers (Alkhalidi et al. 2016). With this setup, an alternating pulsation was achieved in a 750 L tank with 0.4 to 2 Hz pulsation frequency. Both investigations showed that the mass transfer and aeration efficiency can be improved depending on the flow rate and pulsation frequency.

However, due to the lack of advanced measurement devices and the fact that the experimental results are from small scales compared to the application in wastewater treatment, the current findings only show the macroscopic effects of dynamic aeration methods. The knowledge of the local, microscopic and transient hydrodynamics is scarce. The dynamic aeration is defined by a limited number of parameters such as the gas flow rate, aeration period/ frequency, pulse width and base flow rate. These parameters influence the hydrodynamic parameters of the multiphase flow. It is expected that the bubble size changes due to pulsations and higher oxygen concentration gradients between pulses are present. Furthermore, the increased gas flow rate during pulses is expected to lead to higher turbulence in the liquid phase. In conclusion, also increased mass transfer is expected.

This study is focused on the sensitivity analysis of the numerical model. The effect of hydrodynamic parameters on oxygen mass transfer during pulsed aeration is investigated. In contrast to previous studies with gas pulsations, the present study is aimed at the application in wastewater treatment. Therefore, we performed numerical simulations for a larger liquid volume with a side length of 0.75 m and a height of up to 4 m. With gas flow rates in the range of 0.75 to 3.0 m^3/h, the superficial gas velocity is in the range of 0.037 to 0.148 cm/s. Furthermore, this study distinguishes from previously published simulations of gas pulsations, because no base gas flow is used as in the investigations of Jia et al. (2011) and Zhou et al. (2013). The dynamic aeration without base flow as simulated in this investigation is expected to be more beneficial on mass transfer. The numerical simulation study was conducted to

characterize the effect of pulsation frequency, bubble size, aeration depth and gas flow rate on the oxygen mass transfer.

MODEL DESCRIPTION and METHODS

CFD modelling

A three-dimensional transient Euler-Euler simulation was used to simulate the mass transfer characteristics of gas-induced pulsed flow and compare it to continuous gas flow conditions. Bubble sizes between 2.0 and 4.0 mm, which are typical for membrane diffusers (Hasanen et al. 2006) were considered in a mono-disperse model. Bubble break-up and coalescence was neglected, because of the unknown behaviour in the pulsed bubble swarms. Three different gas flow rates were set in the simulation. For the test geometry, they are in a range, which is applicable for wastewater treatment. Low pulsation frequencies in the range of 0.1 to 4 Hz were used, due to their possible application in wastewater treatment. The frequency range is chosen to include the frequencies that have been experimentally investigated in small scale setups before (Alkhalidi et al. 2016) and is extended also to lower and higher frequencies.

For the determination of the mass transfer, the Two-Resistance model in ANSYS CFX was utilised. Both phases are considered as a mixture of two components and for the variable mass fraction of oxygen the scalar transport equation is solved:

$$\frac{\partial(\rho_k \alpha_k x_{O_2,k})}{\partial t} + \nabla \cdot (\rho_k \alpha_k x_{O_2,k} \vec{u}_k) = \nabla \cdot (\alpha_k \left(\rho_k D_{O_2,k} + \frac{\mu_{T,k}}{Sc_{T,k}} \right) \nabla x_{O_2,k}) \pm \Gamma_{O_2,gl} \qquad 1$$

The turbulent Schmidt number $Sc_{T,K}$ is set to the standard value of 0.9 and the oxygen inter-phase mass transfer source term $\Gamma_{O_2,gl}$ was calculated by:

$$\frac{\partial x_{O_2}}{\partial t} = \Gamma_{O_2,gl} = k_L a_g \left[(\rho_l x^*_{o,l} - (\rho_l x_{o,l}) \right] \qquad 2$$

The volumetric mass transfer coefficient and the specific interfacial area were determined according to

$$k_L = 2\sqrt{\frac{D_L}{\pi}}\left(\frac{\varepsilon}{\nu_L}\right)^{0.25} \quad 3$$

and

$$a_g = 6\,\alpha_g/d_B \quad 4$$

The model for the volumetric mass transfer coefficient is derived from Higbie's penetration theory and commonly used in numerical simulations and experimental investigations of bubbly flows (Zhou et al. 2013; Dhanasekharan et al. 2005; Waghmere et al. 2007). The interfacial area is calculated with equation 4 according to Deckwer (1992).

Each of the both phases contains a constrained component to balance the mass fraction sum (equations 5 and 6). In the gaseous phase nitrogen and in the liquid phase water were considered as constraint components.

$$x_{O_2,g} + x_{N_2,g} = 1 \quad 5$$

$$x_{O_2,l} + x_{w,l} = 1 \quad 6$$

For the interphase forces and turbulence modelling the so-called baseline model with mono-disperse setup was used. A compilation of the employed models can be found in Table 1. These interphase forces define the coupling between the liquid and the gaseous phase. The drag force models the friction between the phases. It determines the rise velocity of the bubbles together with the lift force and play an important role in all relative movements of the two phases. The virtual mass force takes in account, that the rising bubble accelerates the surrounding liquid. The inertia of the liquid phase mass encountered by the accelerating bubbles exerts a virtual mass force on the bubbles. The lift force acts lateral to the flow direction and reflects the complex interaction between bubbles and the liquid velocity field. The turbulent dispersion

force describes the effect of turbulent velocity fluctuations and their action on the spatial dispersion of the gaseous phase.

Table 1: Compilation of interphase forces and turbulence force used

Force/Model	Ref
Drag force	Ishii und Zuber (1979)
Lift force	Tomiyama (2002)
Virtual mass force	C_{VM}= 0.5
Turbulent dispersion force	Favre Averaged Drag Force
Turbulence of gas phase	Dispersed Phase Zero Equation model
Turbulence of liquid phase	SST model with automatic wall function
Bubble Induced Turbulence	Additional source terms in the k, ω equations of the SST model.
Turbulent viscosity	Rzehak (2013)

Numerical implementation and geometry

The CFD code presented before was numerically solved by ANSYS CFX 18.0. The high-resolution discretization of the partial and ordinary differential equations and a coupled volume fraction algorithm were used. They couple the equation for velocity, pressure and volume fraction. The two simulated test basins have a square base with a side length of 0.75 m and a height of 2 m and 4 m, respectively. A structured Cartesian grid with 72000 and respectively 144000 cells was applied to the test geometries, which results in a cell size of 25 x 25 x 25 mm. The test geometry is presented in Figure 1. The time step was set to 0.1 s with a total simulated time of 15000 s. The convergence criteria were specified with the root mean square level (RMS) of $1 \cdot 10^{-4}$ for all variables.

The gas inlet was modelled in the centre of bottom of the test geometry with a size of 0.25 x 0.25 m. The oxygen mass fraction of the gas at the inlet was set to 23.1%. The bubble size at the inlet was set to 2.0, 3.2 and respectively 4.0 mm depending on the simulation case. The outlet was the entire area on top of the geometry with a degassing condition for the disperse phase and free slip condition for the continuous phase. The boundary condition of the test geometry walls was set to no slip. At the beginning of the transient simulation, the oxygen mass fraction in the liquid phase was 0%.

The gas mass flow rates for the pulsed aeration were implemented with rectangular waves for the whole frequency range of 0.1 to 4 Hz. This frequency range is close to the small scale experimental investigations of Alkhalidi et al. (2016). The average gas mass flow rate of continuous and pulsed aeration was identical in all cases. This resulted in higher maximum mass flow rates in the pulsed aeration regimes, as shown in Figure 2. A compilation of the varied parameters in the simulations is listed in Table 2.

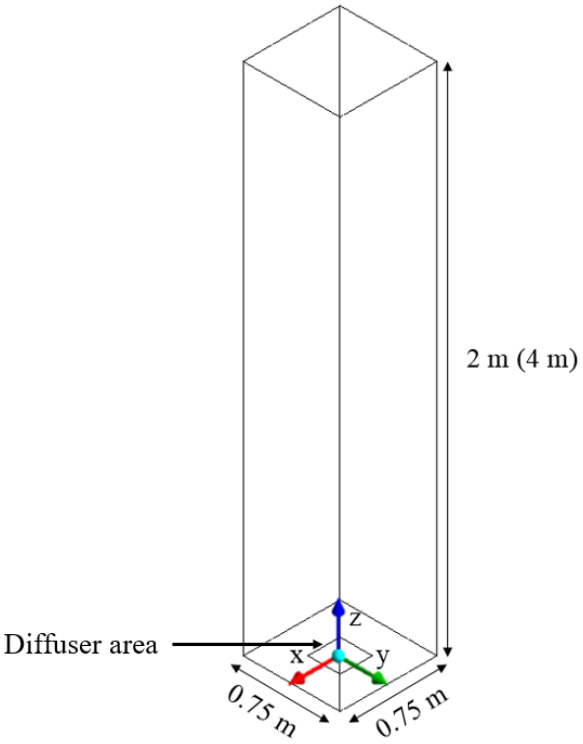

Figure 1: Test geometry with dimensions and origin of coordinates.

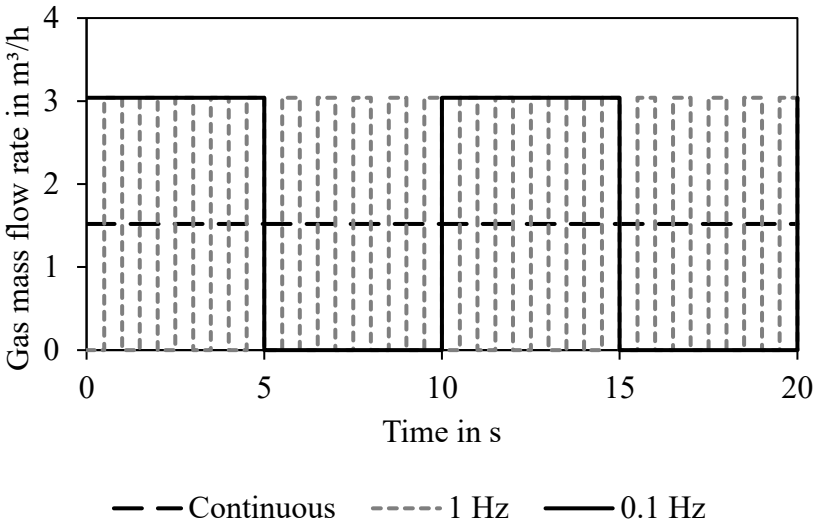

Figure 2: Example of continuous and dynamic gas mass flow rates over time.

Table 2: Simulation parameters

Parameter	Used values
Gas flow rate	0.75; 1.50; 3.00 m³/h
Pulsation frequency	0 Hz (continuous aeration); 0.1; 0.125; 0.25; 0.5; 1; 2; 4 Hz
Aeration depth	2; 4 m
Bubble size	2.0; 3.2; 4.0 mm

Determination of volumetric mass transfer coefficient

To evaluate the effect of dynamic aeration on oxygen mass transfer, the volumetric mass transfer coefficient $k_L a$ is determined by the gassing out method. This standard method in wastewater treatment applications evaluates the $k_L a$ from time-dependent oxygen concentration profiles (DWA M 209). Therefore, the simulations start with a dissolved oxygen concentration of zero. Due to aeration with air, the oxygen concentration rises over time based on the gas-liquid mass transfer as shown in Figure 3.

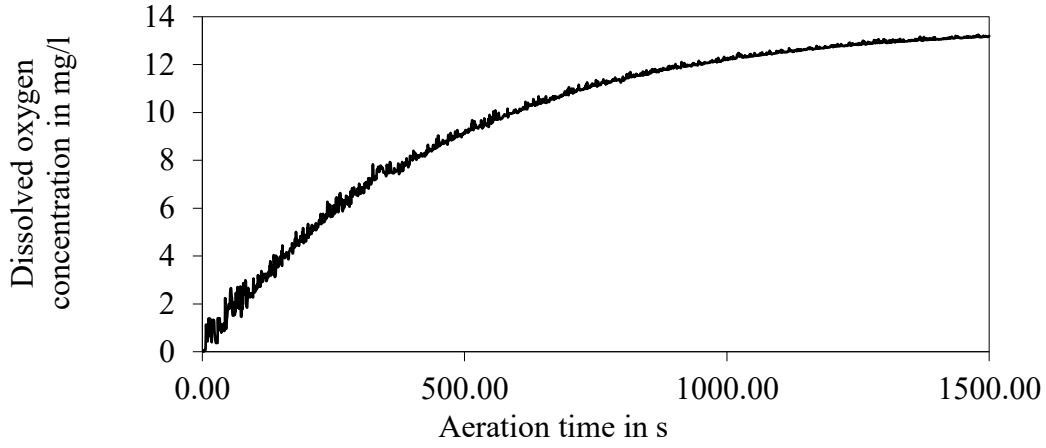

Figure 3: Typical oxygen concentration curve during absorption test for determination of volumetric mass transfer coefficients.

Under the assumption of ideal mixing, negligible nitrogen counter diffusion, constant interfacial area, no significant change of oxygen in the gas phase and with a fast oxygen probe the volumetric mass transfer coefficient can be evaluated with the following expression:

$$\frac{dC}{dt} = k_L a \cdot (C_S - C) \qquad 7$$

The mass transfer is driven by the concentration gradient between bulk concentration C and the saturation concentration C_S. The ODE in equation 7 is solved by separation of variables with the integration boundaries of $C_{start} = C_0$ and $C_{end} = C_t$ for the oxygen concentration and $t_{start} = 0$ and $t_{end} = t$ for the time to get equation 8.

$$C_t = C_S - (C_S - C_0) \cdot e^{-k_L a_T \cdot t} \qquad 8$$

For the evaluation of $k_L a$ from time-dependent oxygen concentration profiles equation 8 is fitted using non-linear regression to the measured oxygen concentrations of the numerical simulations.

The $k_L a$ is used to calculate the standard oxygen mass transfer rate (SOTR), which is required for the determination of the standard oxygen transfer efficiency (SOTE):

$$SOTR = V \cdot k_L a \cdot C_S \qquad 9$$

$$SOTE = \frac{SOTR}{\dot{m}_{O_2}} \cdot 100\% \qquad 10$$

The oxygen mass flow rate is calculated from

$$\dot{m}_{O_2} = \rho_{O_2} C_{O_2} \dot{V}_{Air} \qquad 10$$

where ρ_{O_2} is the oxygen density at standard conditions, $C_{O_2} = 20.95\%$ is the volumetric oxygen concentration in air and $\dot{V}_{Air}$ is the supplied air flow rate. The SOTE enables the comparison of oxygen mass transfer results from setups with different geometries.

RESULTS

The numerical simulations were conducted with variation of the parameters presented in Table 2. The results are divided into the effects of the various parameters on the oxygen mass transfer. Whereby, the results of the 2 m test geometry are presented first. The influence of the liquid level is shown in its own paragraph.

Effect of pulsation frequency

Figure 4 shows the local dissolved oxygen concentration curve after the start of the simulation at the centre of the column for a pulsed aeration with 0.125 Hz and in comparison to continuous aeration for the same average gas mass flow rate. In the dynamic aeration regimes the dissolved oxygen concentration profile shows high peaks in the moment when the gas flow reaches the column's centre. This is visible in the gas hold-up at the monitor point, which is depicted in **Fehler! Verweisquelle konnte nicht gefunden werden.** as well. In the case of dynamic aeration, the dissolved oxygen concentration follows the gas hold-up curve.

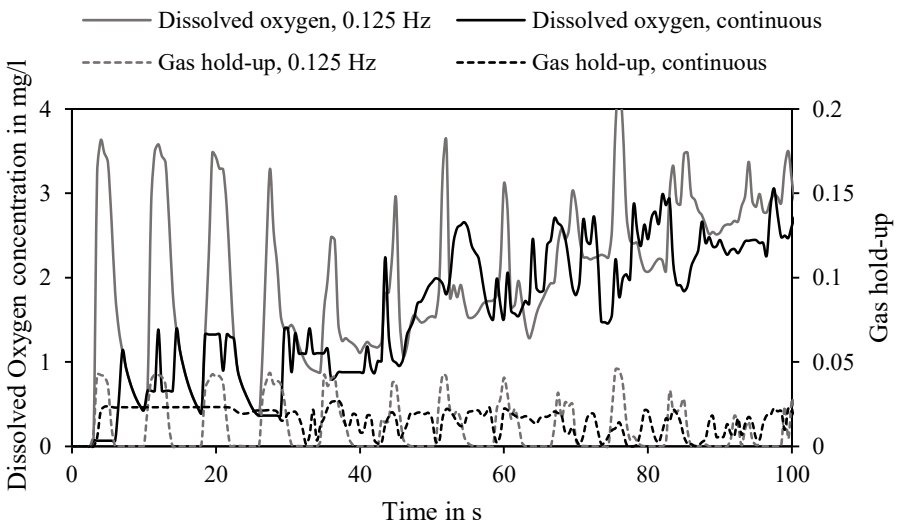

Figure 4: Dissolved oxygen concentration and local gas hold-up for continuous and dynamic aeration measured at a monitor point in the centre of the test geometry.

There is a slight delay in the occurrence of the concentration and volume fraction peaks due to mass transfer and mixing in the liquid. For continuous aeration, the gas hold-up at the monitor point is fluctuating less. Fluctuations only occur due to bubble plume oscillations. Since the liquid oxygen mass fraction is 0 in the beginning of the simulation, the gas pulses with their high gas hold-up result in high dissolved oxygen concentration peaks due the stagnant liquid phase and high concentration gradients. As visible in Figure 5, the liquid velocity increases after the first pulses and the distribution of dissolved oxygen is improved. With continuous aeration, the dissolved oxygen concentration in the centre region is always higher in comparison to the surrounding liquid volume. In pulsed aeration, the gas flow is discontinuous and the centre region has a lower dissolved oxygen concentration compared to the region closer to the wall. This is visible in Figure 5 at 10s. A new pulse of gas rises into an area with lower dissolved oxygen concentration. The higher local oxygen concentrations lead to high oxygen mass transfer. The local peaks in oxygen concentration in pulsed aeration with 0.125 Hz in Figure 4 indicate this as well.

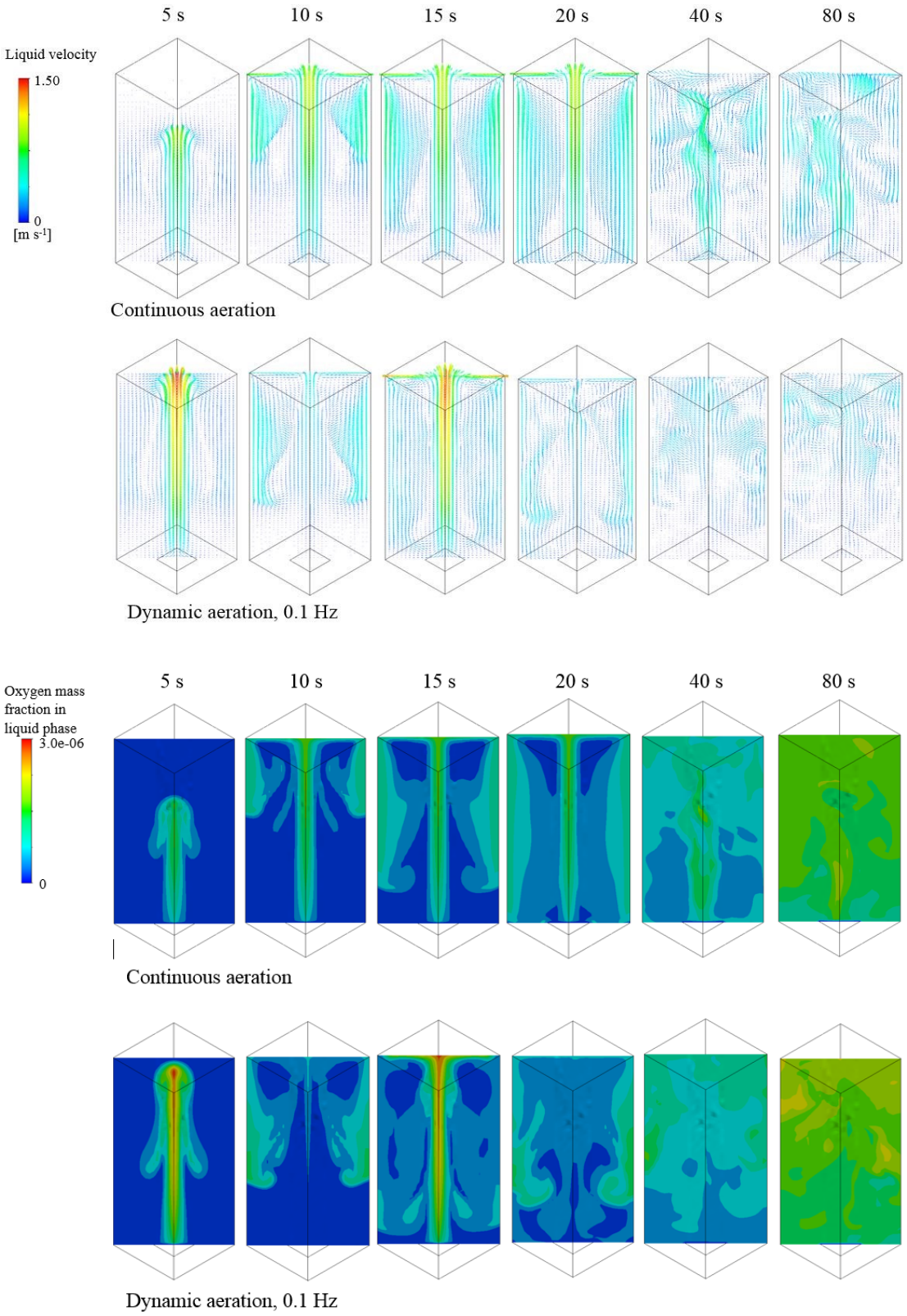

Figure 5: Liquid velocity fields (top) and dissolved oxygen mass fraction (bottom) for continuous aeration and pulsation with 0.1 Hz frequency and mean gas flow rate of 1.5 m³/h.

For the case with a gas mass flow rate of 1.5 m³/h, Figure 6 presents the volumetric mass transfer rates for continuous and dynamic aeration that have been determined by Equation 8 from the oxygen concentration curves. Furthermore, the increase of the k_La in comparison to the continuous case in percent is depicted as curve. The pulsations with 2 and 4 Hz show the highest k_La values among the tested pulsations. An increase of about 24% in volumetric mass transfer coefficient was determined for the pulsation with 2 Hz.

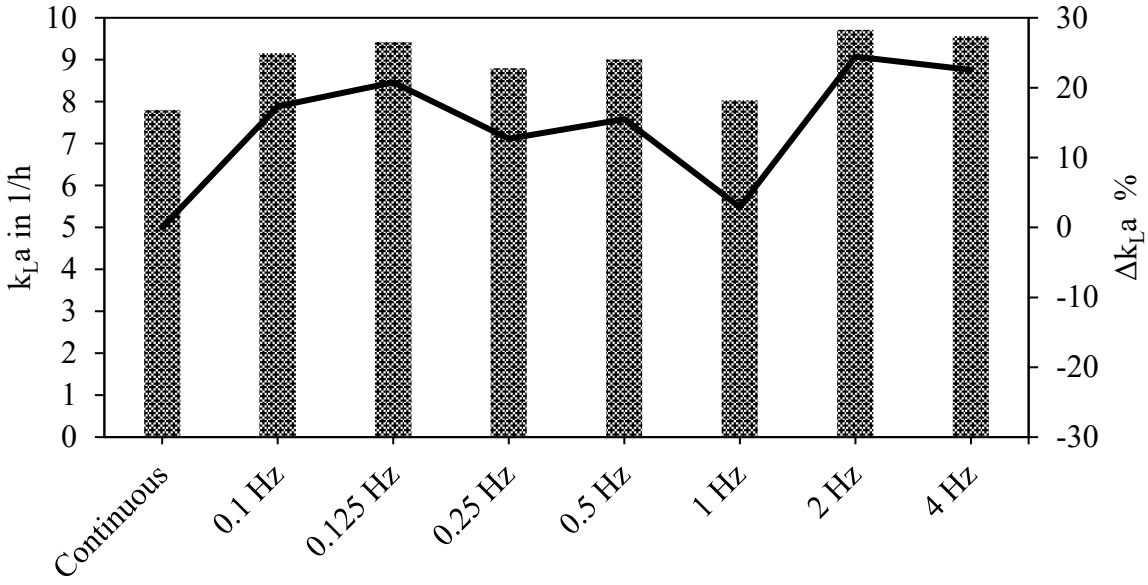

Figure 6: Comparison of volumetric mass transfer coefficients (bar chart) and its relative changes (line plot) for continuous aeration and dynamic aeration in the range of 0.1 to 4 Hz with an average gas mass flow rate of 1.5 m³/h.

The volumetric mass transfer coefficient is derived from the product of Equations 3 and 4. Gas hold-up and the turbulent eddy dissipations are the influencing parameters of the mass transfer coefficient, despite the fixed parameters in these equations. A comparison of time averaged horizontal turbulent eddy dissipation profiles for different simulations is shown in Figure 7. Only the pulsation with 4 Hz frequency surpasses the continuous aeration in the maximum turbulent eddy dissipation in the centre of the test geometry. Low pulsation frequencies result in an eddy dissipation profile, which is more uniformly distributed. The gas phase distribution

in this area is improved for the low pulsation frequencies as well, as shown in Figure 8. However, the effect of the turbulent eddy dissipation on the volumetric mass transfer coefficient is smaller than the effect of the gas hold-up. This can be found in equations 3 and 4, where the gas holdup contributes with a factor of 6 to the interfacial area while the eddy dissipation increases k_L only with its fourth root.

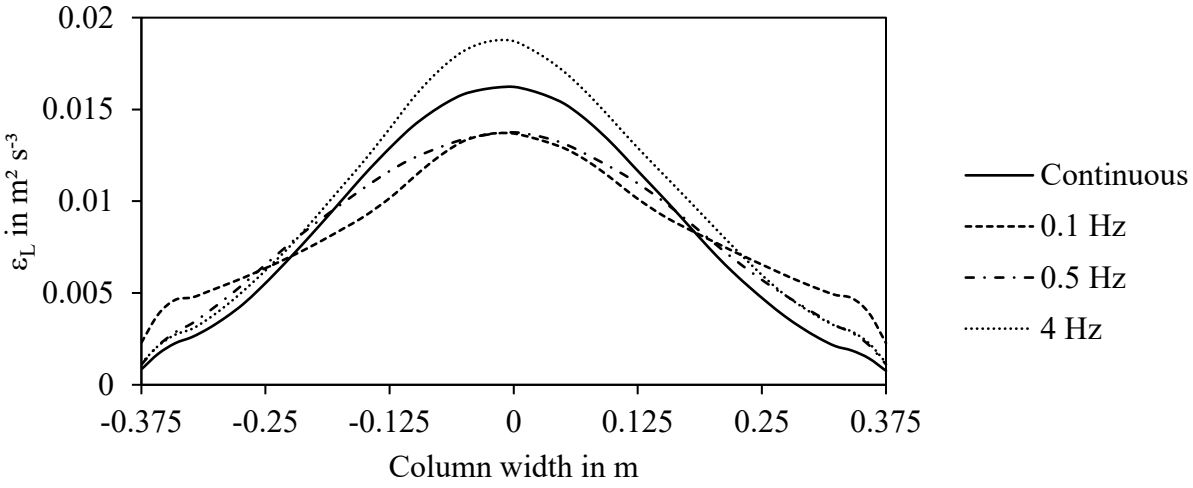

Figure 7: Effect of pulsation frequency on time averaged turbulent eddy dissipation (x = 0, z = 1.5 m).

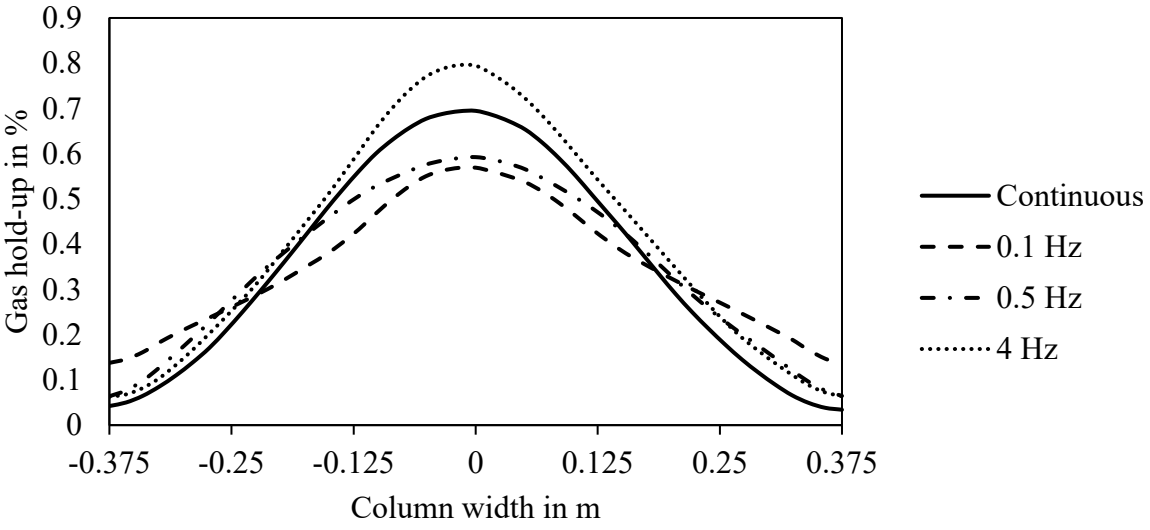

Figure 8: Effect of pulsation frequency on time averaged gas hold-up at 1.5 m liquid height.

Figure 9 shows the mean turbulent eddy dissipation and the gas hold-up for all simulations with 1.5 m³/h average flow rate. The gas hold-up curve correlates with the mass transfer curve in Figure 6. The drop in gas hold-up for 1 Hz pulsations indicates unfavourable macroscopic effects, which occur in this case. These macroscopic effects include higher liquid velocities in the centre region, where the main part of the air bubbles rises as depicted in figure 10. The higher velocities lead to lower residence times and therefore to lower gas hold-up. Only the faster pulsations have a positive effect on the mean turbulent eddy dissipation in comparison with the continuous aeration.

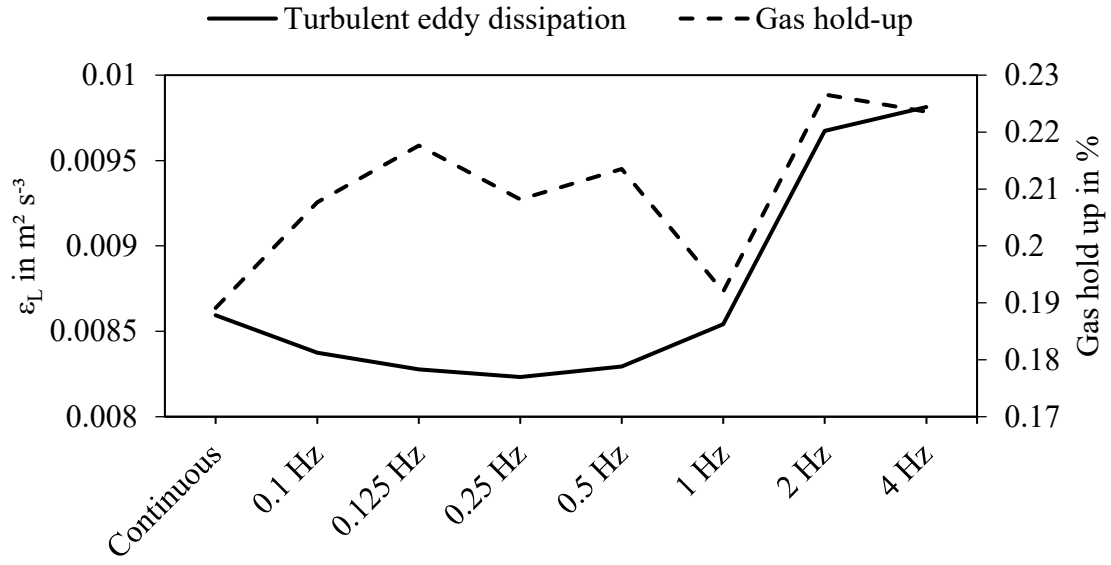

Figure 9: Mean turbulent eddy dissipation at a liquid height of 1.5 m and average gas hold up for simulations with mean flow rates of 1.5 m³/h.

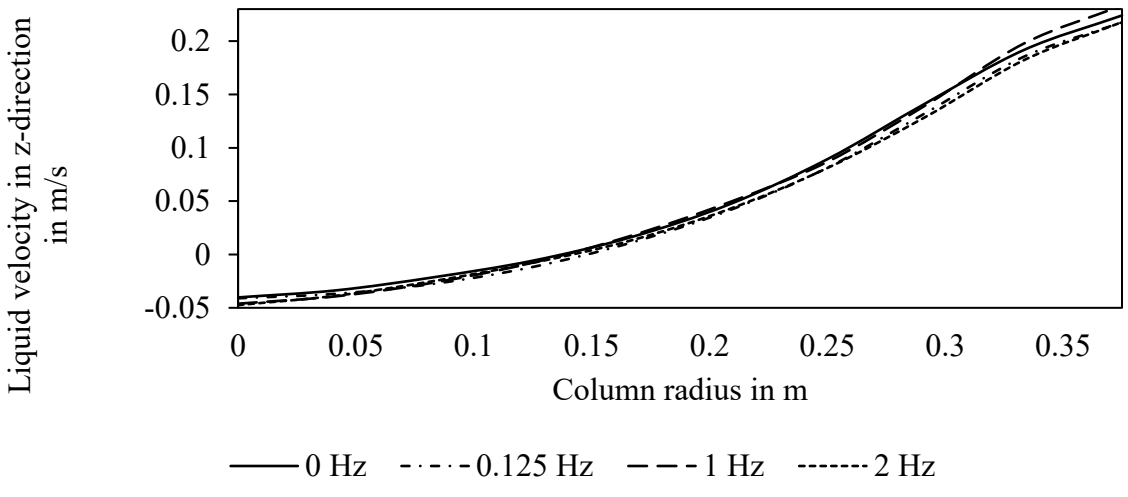

Figure 10: Radial profile of the time-averaged liquid velocity at 0.5 m height in 2 m geometry with 3.2 mm bubbles.

Effect of bubble size

According to the literature, smaller bubbles lead to higher interfacial areas and increase the mass transfer coefficient (Motarjemi and Jameson 1978). The simulations with the bubble sizes of 2.0, 3.2 and 4.0 mm were run to determine if the effect of dynamic aeration is still present with varied bubble sizes. The simulations were conducted with uniform bubble size distributions due to unknown bubble coalescence and break-up behaviour. Figure 11 shows the effect of different bubble sizes on oxygen mass transfer in pulsed aeration for the test geometry with 2 m liquid height. As expected, the lowest bubble size achieves the highest mass transfer rates, whereas simulations with 4.0 mm bubbles result in low mass transfer rates.

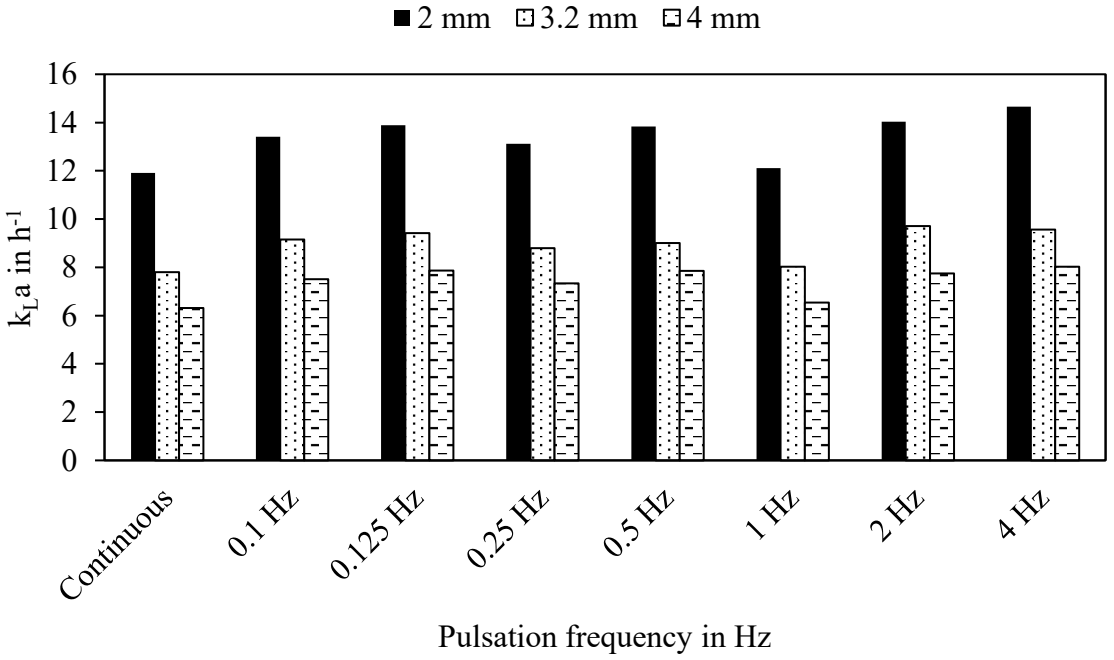

Figure 11: Effect of bubble size on mass transfer rates with pulsation frequencies ranging from 0.1 Hz to 4 Hz.

Due to the uniform bubble size setup, the gas hold-up is directly affected by the bubble size as depicted in Figure 12. With higher gas hold-up and decreased bubble size, the interfacial area calculated with equation 4 raises and thereby the mass transfer rates.

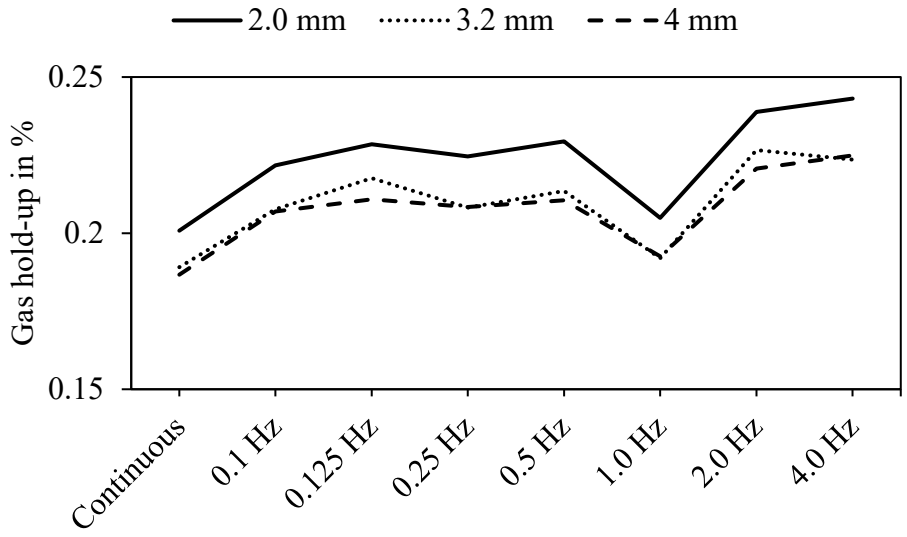

Figure 12: Effect of bubble size on gas hold-up with pulsation frequencies ranging from 0.1 Hz to 4 Hz.

Effect of mass flow amplitude

As typical for bubbly flows, the mass transfer depends on the gas mass flow rate. Figure 13 shows the dependency of the volumetric mass transfer coefficient on the gas mass flow rate. In every case, the mass transfer rates are higher for increased flow rates.

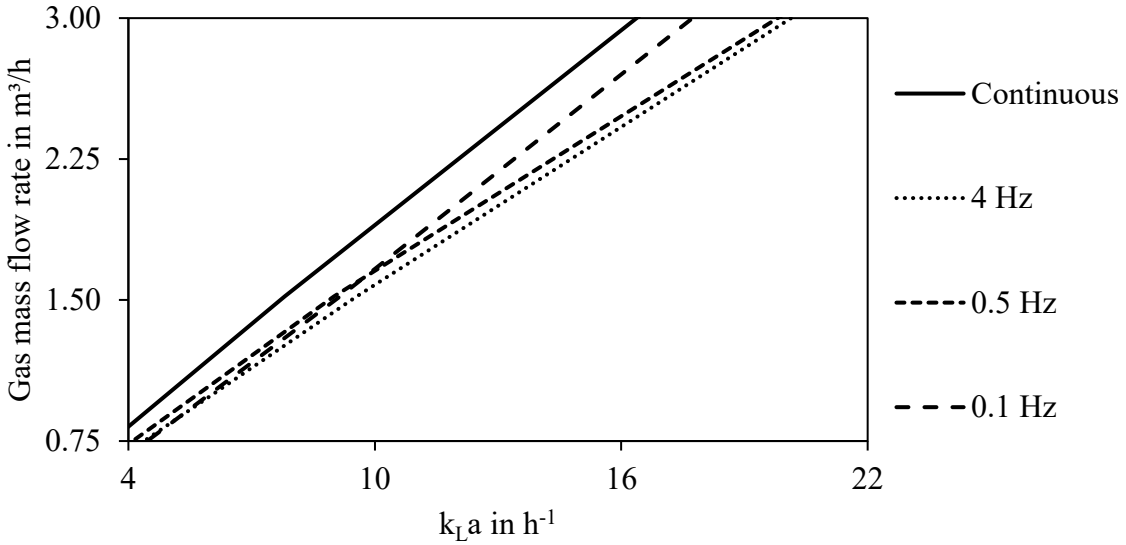

Figure 13: Inverted dependency of mass transfer rate on gas mass flow rate with 2 m liquid level (with bubble size of 3.2 mm).

Since the simulations use a mono-disperse setup, the higher gas flow rate directly correlates with higher interfacial area due to higher gas hold-up. Figure 14 shows the gas hold-up for a pulsed aeration with the three flow rates.

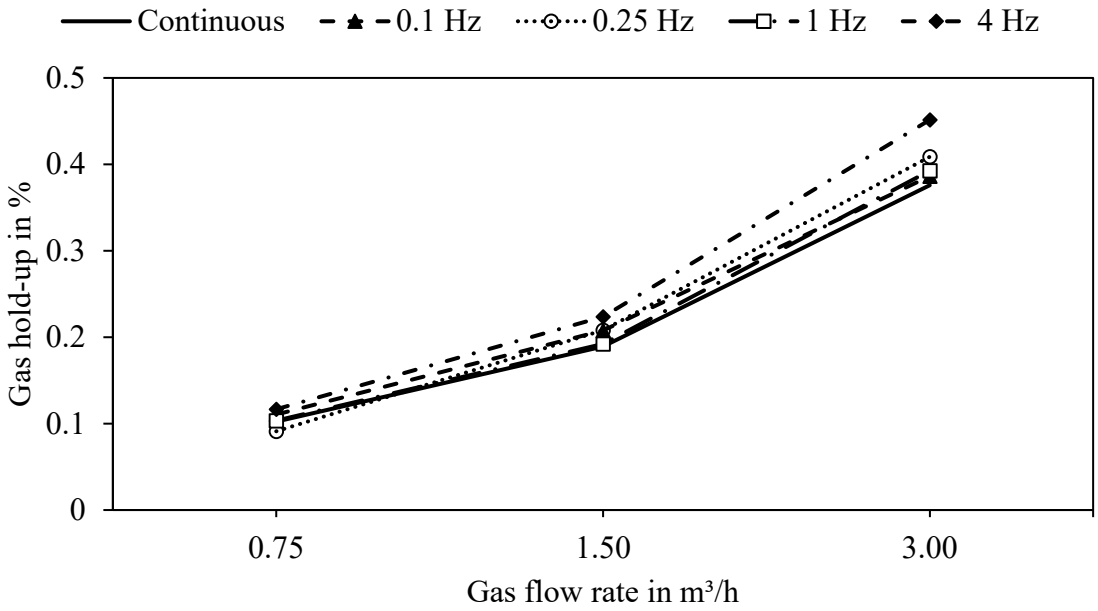

Figure 14: Comparison of gas hold-up with 0.75, 1.5 and 3.0 m³/h gas flow rate.

The k_La for the continuously aerated case is the lowest for the cases 1.5 and 3.0 m³/h gas flow rate. The low k_La at 0.75 m³/h and 0.25 Hz pulsed aeration shows that the pulsations can decrease the gas hold-up as well. Whereas with the other pulsation regimes higher mass transfer coefficients are achieved. According to the graphs in Figure 13, it is possible to reach the equivalent mass transfer coefficients to continuous aeration with lower gas mass flow rates in the pulsed aeration. Whilst the continuously aerated test geometry achieves a k_La of 7.8 h^{-1} at 1.5 m³/h, the same mass transfer coefficient is possible with only 1.25 m³/h with a pulsation frequency of 4 Hz. The gas flow rate can be reduced by almost 16% while transferring the same

amount of oxygen into the aeration basin.

Effect of aeration depth

The effects of pulsed aeration are still significant, when the liquid level is doubled. The simulations with 4 m aeration depth show a similar behaviour in terms of oxygen mass transfer. However, the relative increase in mass transfer rates is lower compared to the continuously aerated case as depicted in Figure 15. Furthermore, the absolute mass transfer rates with higher aeration depths were slightly lower for all aeration regimes. The lower oxygen transfer rates in deeper aeration basins was reported in literature before (Wagner and Pöpel 1998). The oxygen transfer is affected by changes in oxygen saturation in the liquid and lower oxygen content in bubbles due to their longer residence time.

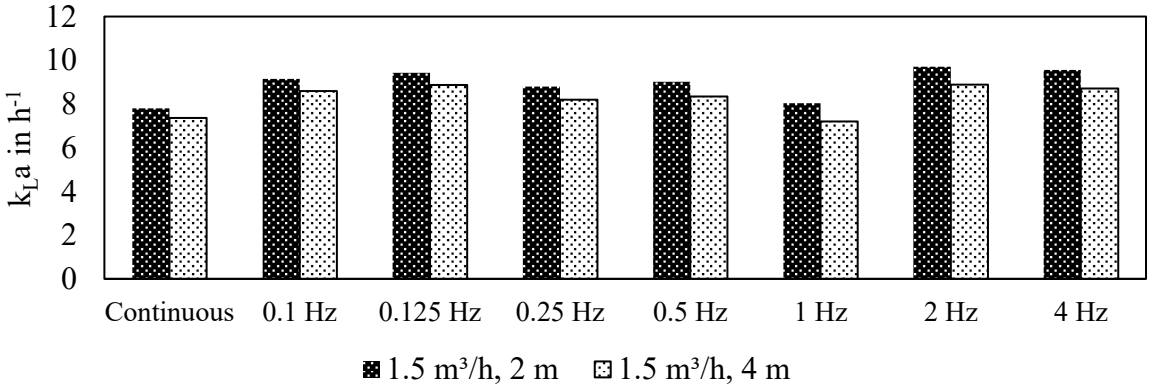

Figure 15: Comparison of mass transfer rates for pulsed and continuous aeration with different aeration depths.

The higher liquid level results in lower liquid velocities. Compared to the 2 m test geometry the bubble rise path is longer. In both cases, the rising bubbles increase the liquid velocity in the centre region and liquid flow is deflected at the liquid surface as depicted in Figure 16. For the smaller geometry, this results in higher average liquid velocities as shown in Figure 16. Therefore, the effect of pulsed aeration is enhanced in smaller geometries.

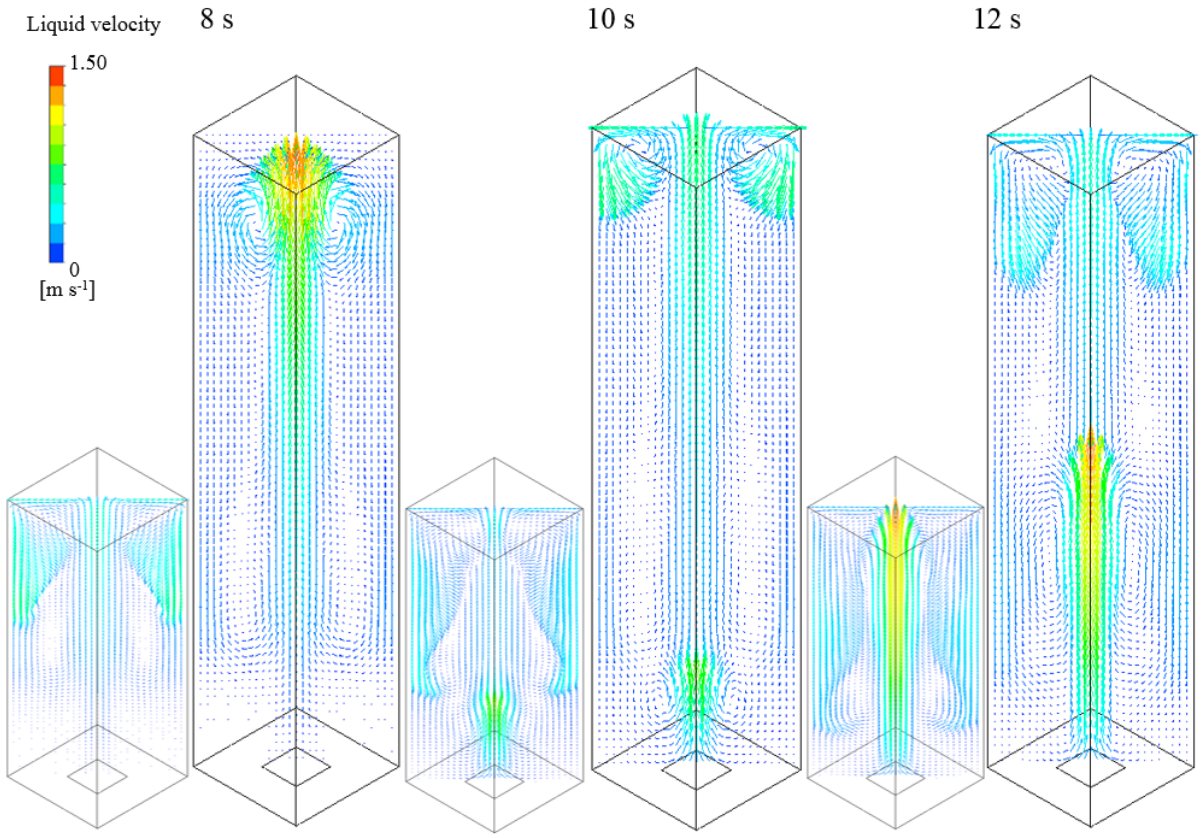

Figure 16: Liquid velocity fields in 2 m and 4 m basins with 0.125 Hz pulsation frequency and 1.5 m³/h gas flow rate.

Figure 17 shows the inverted dependency of the mass transfer rate from the mean gas flow rate for the cases with 4 m liquid height. With this liquid height, which is more common for wastewater applications, energy savings due to a possible reduction of the gas flow rate in the range of 14.6% are achievable with 4 Hz pulsations. This is close to the result achieved in the 2 m test geometry and is a hint to the amount of energy, which can be saved by employing dynamic aeration in the aeration basins of wastewater treatment.

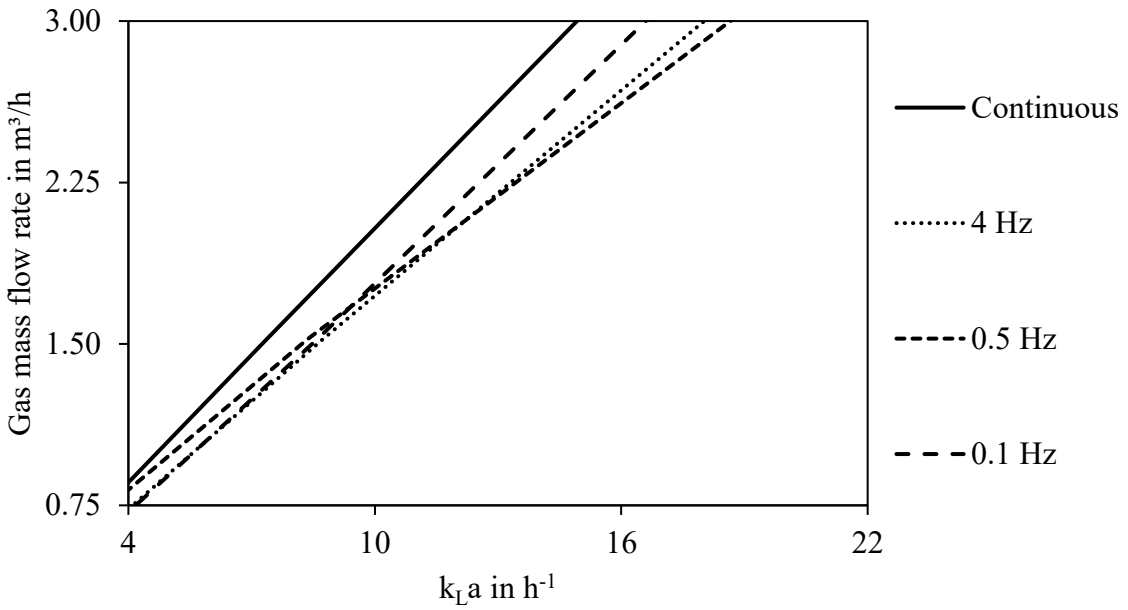

Figure 17: Inverted dependency of mass transfer rate on gas mass flow rate with 4 m liquid level.

Comparison of simulation with experimental results

The oxygen transfer efficiencies derived from the volumetric mass transfer coefficients of the numerical simulations with 4 m aeration depth and the experiments of Alkhalidi et al. (2016) using equation 10 are depicted in figure 18. The SOTE of the numerical simulations and the experiments are in a comparable range. Furthermore, the trend of the SOTE values across the frequency range is very similar. Decreased SOTE for pulsation frequencies of 0.25 Hz and 1 Hz observed in the experiment are also reflected in the simulations. This provides evidence for the validity of the simplified numerical simulations for sensitivity analysis of the hydrodynamic parameters on the oxygen mass transfer under pulsed aeration. Moreover, the scalability of the pulsation effects to relevant aeration depths is verified by this result.

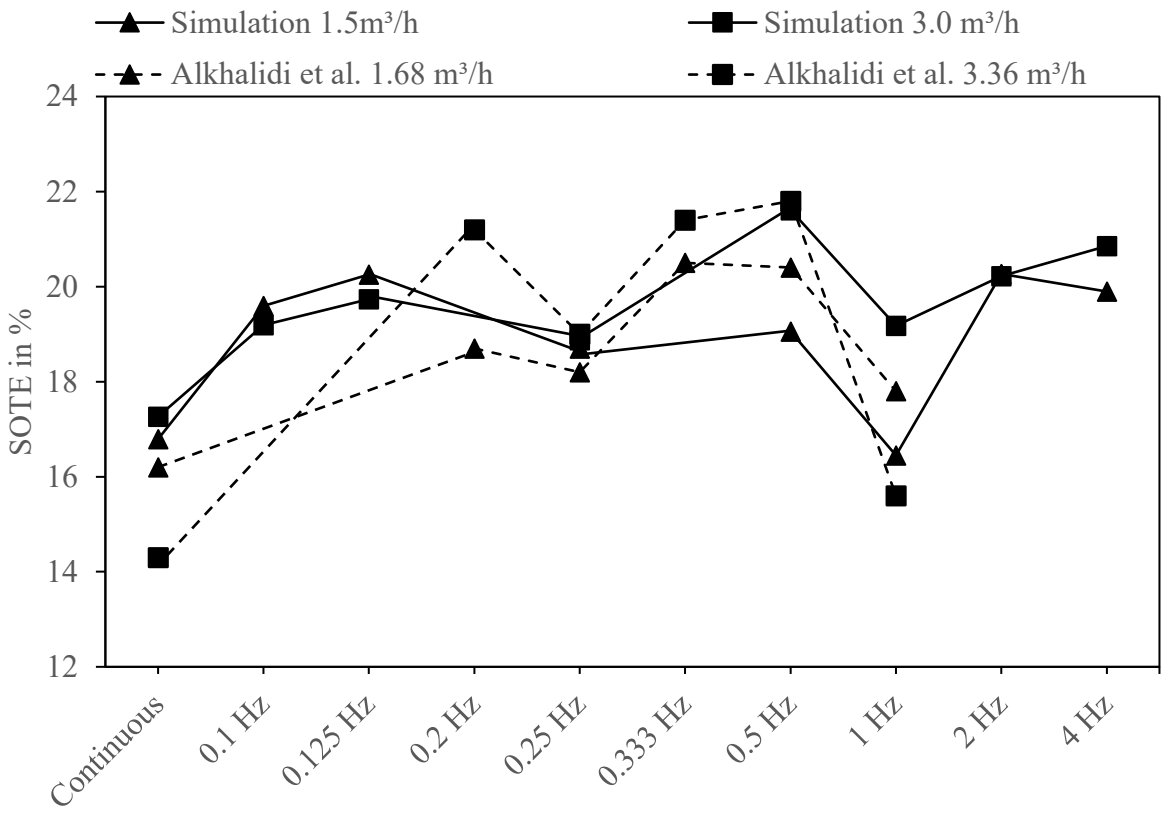

Figure 18: Comparison of the standard oxygen transfer efficiencies (SOTE) for the investigated pulsation frequencies and gas flow rates from numerical simulations of the current study (aeration depth 4 m) and experimental results of Alkhalidi et al. (2016).

CONCLUSIONS

In this study, the effect of dynamic aeration in form of pulsed gas flow on the oxygen mass transfer is investigated. The investigation focuses on the application of the dynamic aeration in wastewater treatment to optimize energy efficiency. Therefore, numerical simulations are run with variation of pulsation frequency, pulsation amplitude, liquid height and bubble size to evaluate their influence on the oxygen mass transfer. The parameter range is chosen to be applicable for the future use in wastewater aeration basins.

It is found that dynamic aeration shows a significant increase of mass transfer rates in the investigated frequency range and mass transfer is raised by up to 24% for pulsations with 2 Hz frequency. Furthermore, the pulsation leads to a higher gas hold-up. The increase in oxygen

transfer rate is verified also with aeration depths of 4 m and bubble sizes in the range of 2.0 to 4.0 mm. The simulation of mean gas flow rates between 0.75 and 3.0 m³/h give a preview of possible energy savings for wastewater treatment. Equivalent volumetric mass transfer rates are achieved with lower gas flow rates for pulsed aeration, which results in lower power consumption of air blowers when dynamic aeration is applied in wastewater treatment. The oxygen transfer efficiencies derived from the simulations are in good agreement with the experimental results from Alkhalidi et al. (2016). This provides evidence for the validity of the simplified numerical method and the scalability of the pulsation effects to relevant aeration depths.

The study shows the possible positive effects on oxygen mass transfer. However, there are still open questions and phenomena that must be investigated in further research. The macroscopic effects of pulsations on the hydrodynamic flow behaviour, which lead to higher gas hold-up must be investigated further. The bubble behaviour under pulsed aeration is unknown so far. This includes the bubble break-up and coalescence and the initial bubble size depending on the pulsation frequency and gas flow rate. This must be investigated in experimental investigations. Furthermore, the mixing behaviour is of interest. It is important to understand the changes in gas hold-up and oxygen concentration gradients in the liquid phase. For the application in wastewater treatment, the mixing behaviour is of high relevance. Sedimentation of particles and flocs must be avoided.

ACKNOWLEDGEMENT

This work was partly founded by AIR LIQUIDES.A. and we would like to thank Dr. Markus Meier (AIR LIQUIDE Forschung und Entwicklung GmbH) for his support.

NOMENCLATURE

a_g	Interfacial area of bubbles, m^{-1}

C	Concentration, kg m^{-3}
C_0	Dissolved oxygen concentration at t=0, kg m^{-3}
C_S	Oxygen saturation concentration, kg m^{-3}
C_t	Dissolved oxygen concentration at time t
C_{vm}	Virtual mass coefficient, dimensionless
d_b	Bubble diameter, m
D_L	Molecular-diffusion coefficient
D_i	Kinematic diffusivity, m^2 s^{-1}
k_L	Liquid side mass transfer coefficient, m s^{-1}
k_La	Volumetric mass transfer coefficient, s^{-1}
$\dot{m}$	Mass flow, kg h^{-1}
$Sc_{T,k}$	Schmidt number, dimensionless
SOTE	Standard oxygen transfer efficiency, %
SOTR	Standard oxygen transfer rate, kg h^{-1}
$\vec{u}_k$	Velocity vector, m s^{-1}
V	Volume of basin, m^3
$\dot{V}_{Air}$	Air volume flow in m^3 h^{-1}
x_i	Mass fraction, dimensionless

Greek letters

α_i	Gas hold-up/ Volume fraction, dimensionless
Γ_i	Mass transfer source term, kg m^{-3} s^{-1}
ε	Turbulent eddy dissipation in m^2 s^{-3}
μ_i	Dynamic viscosity, Pa s
ν_i	Kinematic viscosity, m^2 s^{-1}
ρ_i	Density, kg m^{-3}
ρ_{O_2}	Oxygen density at standard conditions in kg m^{-3}
$C_{S,20}$	Oxygen saturation concentration at T = 20 °C and p = 1013 hPa

Subscripts

g	Gas phase
L, l	Liquid phase
N_2	Nitrogen
O_2	Oxygen
w	Water

REFERENCES

Alkhalidi, A. A., Al Ba'ba'a, H. B., & Amano, R. S. (2016). Wave generation in subsurface aeration system: a new approach to enhance mixing in aeration tank in wastewater treatment. Desalination and Water Treatment, 57(56), 27144-27151.

DWA-M 209 (2007). Messung der Sauerstoffzufuhr von Belüftungseinrichtungen in Belebungsanlagen in Reinwasser und in belebtem Schlamm (April 2007). DWA Deutsche Vereinigung für Wasserwirtschaft, Abwasser und Abfall e. V.

Deckwer, W. D. (1992). *Bubble column reactors* (Vol. 200). R. W. Field (Ed.). New York: Wiley.

Dhanasekharan, K. M., Sanyal, J., Jain, A., & Haidari, A. (2005). A generalized approach to

model oxygen transfer in bioreactors using population balances and computational fluid dynamics. *Chemical Engineering Science*, *60*(1), 213-218.
Elbing, B. R., Still, A. L., & Ghajar, A. J. (2016). Review of bubble column reactors with vibration. Industrial & Engineering Chemistry Research, 55(2), 385-403.
Fricke, K. (2009). Energieeffizienz kommunaler Kläranlagen. Umweltbundesamt Deutschland: Dessau-Roßlau.
Hasanen, A., Orivuori, P., & Aittamaa, J. (2006). Measurements of local bubble size distributions from various flexible membrane diffusers. *Chemical Engineering and Processing: Process Intensification*, 45(4), 291-302.
Ishii, M., & Zuber, N. (1979). Drag coefficient and relative velocity in bubbly, droplet or particulate flows. AIChE Journal, 25(5), 843-855.
Jia, X., Yuan, Q., Wen, J., & Feng, W. (2011). Fluid flow modeling of a gas-induced pulsating flow bubble column. *Chemical and biochemical engineering quarterly*, *25*(1), 27-36.
Motarjemi M. and Jameson G. (1978). Mass transfer from very small bubbles—the optimum bubble size for aeration. *Chemical Engineering Science* **33**(11), 1415-23.
OECD, Water-Energy Nexus, in World Energy Outlook 2016, OECD Publishing, Paris, 2016. https://doi.org/10.1787/weo-2016-11-en.
Pöpel J., Wagner M. (1994). Theorie und Praxis von Sauerstoffeintrag und –ertrag in tiefen Belebungsbecken. In: 5. Hannoversche Industrieabwassertagung . Veröffentlichungen des Institutes für Siedlungswasserwirtschaft und Abfalltechnik der Universität Hannover. Heft 87, ISBN 3-921421-16-0.
Pöpel J, Wagner M, Weidmann F. (1998). Sauerstoffeintrag und –ertrag in tiefen Belebungsbecken. Schriftreihe WAR, Nr. 4, Techn. Hochschule Darmstadt.
Rzehak, R., Liao, Y., Lucas, D., & Krepper, E. (2013). Baseline model for CFD of dispersed bubbly flow. In *15th International Topical Meeting on Nuclear Reactor Thermal-hydraulics, NURETH-15, Pisa, Italy, May* (pp. 12-17).
Tomiyama, A., Tamai, H., Zun, I., & Hosokawa, S. (2002). Transverse migration of single bubbles in simple shear flows. *Chemical Engineering Science*, *57*(11), 1849-1858.
Waghmare, Y. G., Knopf, F. C., & Rice, R. G. (2007). The Bjerknes effect: Explaining pulsed-flow behavior in bubble columns. *AIChE journal*, *53*(7), 1678-1686.
Xu, P & Shan, J & Jin, X & Yu, J & Sun, Y & Zhang, J. (2015). Performance of impulse-type fine bubble aerator. Chinese Journal of Environmental Engineering. 9. 4287-4292.
Zhou, Z., Yuan, Q., Jia, X., Feng, W., & Wen, J. (2013). Experimental Study and CFD Simulation ofMass TransferCharacteristics of a Gas-Induced Pulsating Flow BubbleColumn. *Chemical and biochemical engineering quarterly*, *27*(2), 167-175.